

Albedos and diameters of three Mars Trojan asteroids

David E. Trilling^{a,*}, Andrew S. Rivkin^b, John A. Stansberry^a, Timothy B. Spahr^c,
Richard A. Crudo^{a,1}, John K. Davies^d

^a Steward Observatory, The University of Arizona, 933 N. Cherry Avenue, Tucson, AZ 85721, USA

^b Applied Physics Laboratory, Johns Hopkins University, 11100 Johns Hopkins Road, Laurel, MD 20723, USA

^c Harvard-Smithsonian Center for Astrophysics, 60 Garden Street, Cambridge, MA 02139, USA

^d UK Astronomy Technology Centre, Blackford Hill, Edinburgh, EH9 3HJ, UK

Received 24 April 2007; revised 20 July 2007

Available online 6 September 2007

Abstract

We observed the Mars Trojan Asteroids (5261) Eureka and (101429) 1998 VF₃₁ and the candidate Mars Trojan 2001 FR₁₂₇ at 11.2 and 18.1 microns using Michelle on the Gemini North telescope. We derive diameters of 1.28, 0.78, and <0.52 km, respectively, with corresponding geometric visible albedos of 0.39, 0.32, and >0.14. The albedos for Eureka and 1998 VF₃₁ are consistent with the taxonomic classes and compositions (S(I)/angritic and S(VII)/achondritic, respectively) and implied histories presented in a companion paper by Rivkin et al. Eureka's surface likely has a relatively high thermal inertia, implying a thin regolith that is consistent with predictions and the small size that we derive.
© 2007 Elsevier Inc. All rights reserved.

Keywords: Trojan asteroids; Infrared observations; Regoliths

1. Introduction

It has been known for nearly a century that a large population of asteroids, known as Trojan asteroids, exists in a 1:1 resonance with Jupiter. Neptune is known to have five Trojan asteroids, but the only rocky planet with known Trojan asteroids is Mars. At present, the number of confirmed Mars Trojan asteroids is four, with a handful of other candidates. All but one orbit in the L₅ (trailing) zone, with 1 in the L₄ (leading) zone.

Mars Trojans can be dynamically stable over the age of the Solar System at inclinations between 12 and 40 degrees (Tabachnik and Evans, 1999; Scholl et al., 2005); all known and candidate Mars Trojans reside in this dynamically stable region of phase space and may therefore be primordial objects. If so, these bodies represent leftover planetesimals from the formation of Mars. It is therefore interesting that there is evidence that suggests a diverse history for these bodies. Rivkin

et al. (2003) obtained visible spectra of the three largest Mars Trojans—(5261) Eureka, (101429) 1998 VF₃₁, and (121514) 1999 UJ₇—and found that Eureka and 1998 VF₃₁ are likely S- or A-class asteroids, whereas 1999 UJ₇ is probably an X-class asteroid. These differing compositions suggest that these asteroids cannot have all formed in the same protostellar disk environment. Rivkin et al. (2007), a companion paper, extend the previous paper, finding that Eureka is angritic (igneous, from an oxidized, carbonaceous chondritic precursor), whereas 1998 VF₃₁ is likely a primitive achondrite (from a reduced origin). The Rivkin spectra represent the total published knowledge of the physical properties of Mars Trojans. Clearly, additional data are needed to characterize these unique objects and unravel the population's history, since Mars Trojans may represent the only known planetesimals that formed interior to the asteroid belt, and are the closest approximations to Earth's building blocks currently known.

We have obtained the first thermal infrared measurements of three Mars Trojan asteroids: (5261) Eureka, (101429) 1998 VF₃₁, and 2001 FR₁₂₇ (this last being unconfirmed as a Mars Trojan due to lack of long-term dynamical integrations). Here we present our data (including some ancillary visible wave-

* Corresponding author. Fax: +1 (520) 621 9555.

E-mail address: trilling@as.arizona.edu (D.E. Trilling).

¹ Present address: Department of Physics, University of Connecticut, U-3046, 2152 Hillside Road, Storrs, CT 06269, USA.

length data); thermal modeling; and the resulting derived diameters and albedos. We briefly discuss the implications of our results, including their general agreement with the taxa presented in Rivkin et al. (2007).

2. Recovery of 2001 FR₁₂₇

2001 FR₁₂₇ was discovered in March 2001, and recovered two weeks later (Tichy et al., 2001). On the basis of this arc, it was identified as a candidate Mars Trojan asteroid. (For simplicity, we refer this body hereafter simply as a Mars Trojan.) However, at the time of our Gemini observations four years later, the positional uncertainty for this object was around 0.67 degrees, far too large to be usefully targeted with Gemini/Michelle (see below), whose field of view is less than 1 arcmin. Before our thermal infrared observations could be carried out, therefore, 2001 FR₁₂₇ needed to be recovered to reduce its positional uncertainty.

We carried out a wide-area recovery program in May and June 2005, using 90prime, the prime focus camera on the University of Arizona/Steward Observatory 90-inch (2.3-m) Bok Telescope on Kitt Peak. 90prime has an array of four 4096 × 4096 CCDs; the sides of the array span 1.16 deg, and the total imaged area of the sky is 1 deg² per pointing (Williams et al., 2004). We imaged a series of overlapping fields along the projected location of 2001 FR₁₂₇. We used a modified version of the Deep Ecliptic Survey data reduction and moving object detection pipeline (Millis et al., 2002; Elliot et al., 2005) to search for 2001 FR₁₂₇, and found it on multiple images. These new astrometric positions (Hergenrother et al., 2005) allowed a substantial refinement of the orbital elements and a consequent reduction in positional uncertainty for 2001 FR₁₂₇. At the time of our Gemini observations of 2001 FR₁₂₇ one month after recovery, the positional uncertainty was less than an arcsecond.

3. Partial lightcurve photometry

In order to detect or place limits on any visible lightcurves, we observed Eureka and 1998 VF₃₁ in V band (predicted magnitudes from Horizons: 18.9 and 20.6, respectively) on 2005 Sep 19 UT with the facility 2K CCD (CCD21) imager on the Steward Observatory Mt. Bigelow 61-inch (1.54-m) Kuiper Telescope. The night was not photometric, so we cannot independently determine the V magnitude of the asteroids. Each asteroid was easily detected in a series of 60-s exposures. 2001 FR₁₂₇ was also attempted, but was too faint (predicted magnitude $V = 22.3$ from Horizons) to be detected in 90-s exposures. Our time baseline was quite short—around 20 min for each of the two detected asteroids. No significant variation in flux from either asteroid was detected (using relative photometry to three comparably bright comparison stars that are nearby in the images). For the bright Eureka, our non-detection of flux variation places a 3σ limit on any lightcurve variation of 0.1 mag over the 20-min observation window. This upper limit is consistent with the Rivkin et al. (2003) measurement (from a different epoch) of a lightcurve amplitude at least 0.15 mag over around 6 h. For the relatively faint 1998 VF₃₁, the 3σ limit on any lightcurve

Table 1
Observing log

| Target | Filter | Obs. time (UT) | Exp. time (s) | Airmass | R (AU) | Δ (AU) | Phase (deg) |
|------------------------|--------|-------------------|------------------|---------|-------------|------------------|----------------|
| Eureka | N' | 9.1675000 | 60 | 1.33 | 1.49 | 0.67 | 34.4 |
| Eureka | Q_a | 9.5359725 | 150 | 1.44 | 1.49 | 0.67 | 34.4 |
| 1998 VF ₃₁ | N' | 10.783750 | 120 | 1.38 | 1.54 | 0.81 | 37.2 |
| 1998 VF ₃₁ | Q_a | 11.152500 | 150 | 1.50 | 1.54 | 0.81 | 37.2 |
| 2001 FR ₁₂₇ | N' | 11.989445 | 120 | 1.21 | 1.69 | 0.93 | 31.4 |
| HD 141992 | N' | 8.7205560 | 15 | 1.07 | ... | ... | ... |
| HD 141992 | Q_a | 8.8315280 | 45 | 1.07 | ... | ... | ... |
| HD 156283 | N' | 11.471250 | 15 | 1.31 | ... | ... | ... |
| HD 158899 | N' | 12.296390 | 15 | 1.46 | ... | ... | ... |
| HD 158899 | Q_a | 12.407080 | 45 | 1.48 | ... | ... | ... |

Note. All observations were made on 2005 Jul 6 (UT), with the exact mid-times indicated. The target asteroids and calibrator stars are given in the top and bottom groups, respectively. The exposure times used to measure object flux are listed here. The total open-shutter times, including both “on” and “off” (unguided) images, were 240 and 300 s for asteroids and 30 and 90 s for calibration stars at N' and Q_a , respectively. However, for all targets, only the “on” (guided) images were used, and for Eureka, the second half of the N' data was poor and not used.

variation is around 1 mag over the 20-min observation window. Both of these non-detections are useful in eliminating the possibility of fast rotations and extreme shapes, which would be suggested by large flux variations over these short time windows.

4. Thermal infrared observations

Mars Trojan Asteroids Eureka, 1998 VF₃₁, and 2001 FR₁₂₇ were observed in queue mode on 2005 Jul 6 (UT) at the Gemini North telescope on Mauna Kea using Michelle, a mid-infrared imager and spectrometer (Glasse et al., 1997). In imaging mode, Michelle has a field of view of 32" × 24", with pixels 0.1 arcsec on a side. We used the N' ($\lambda_c = 11.2 \mu\text{m}$, $\Delta\lambda = 2.4 \mu\text{m}$) and Q_a ($\lambda_c = 18.1 \mu\text{m}$, $\Delta\lambda = 1.9 \mu\text{m}$) filters (see Table 1 for the observing log). The telescope was tracked at asteroid (non-sidereal) rates.

We employed the standard chop–nod strategy in which the telescope secondary chops (several Hertz) and the telescope nods (few times a minute) between nearby (8 arcsec) pointings in order to subtract out the thermal background from the telescope and atmosphere. The data was processed using the `midir` package of the Gemini IRAF package.² The `mirreduce` task conveniently performs all the standard tasks of reorganizing data structures and stacking the chop–nod images to produce final double-differenced images. In each image stack for this program only a single target appears, at very close to its predicted location, so there is no confusion as to whether the measured source is the targeted source. The exceptions are the N' image of 2001 FR₁₂₇ and the Q_a image of 1998 VF₃₁, in which no sources are evident at all; we derive upper limits to the fluxes for these two observations, as described below. In all cases, the images in the “off” positions are unguided and some-

² Available at <http://www.gemini.edu/sciops/data/dataSoftware.html>.

Table 2
Photometry and modeling results

| Target | H (mag) | V (mag) | N' (mJy) | Q_a (mJy) | Albedo | Diameter (km) |
|------------------------|--------------|--------------|---------------|----------------|------------------------|------------------------|
| Eureka | 16.1 | 17.51 | 21.7(2.8) | 30.8(4.8) | $0.39^{+0.18}_{-0.13}$ | $1.28^{+0.08}_{-0.06}$ |
| 1998 VF ₃₁ | 17.4 | 19.38 | 5.1(0.9) | <15.4 | $0.32^{+0.18}_{-0.11}$ | 0.78 ± 0.06 |
| 2001 FR ₁₂₇ | 18.9 | 21.21 | <1.53 | ... | >0.14 | <0.52 |

Note. H magnitudes; V magnitudes at time of Michelle observations, from Horizons; measured fluxes at the isophotal wavelengths of 11.52 and 18.26 μm for N' and Q_a , respectively; and derived physical properties (using the modified STM). The uncertainty in H (and therefore V) is taken to be 0.3 mag. The 1σ errors for our derived albedos and diameters are given. No observation was made of 2001 FR₁₂₇ at Q_a . These STM model results use $\eta = 1.3$. We used the following N' fluxes for photometric calibration: HD 141992, 13.586 Jy; HD 156283, 35.096 Jy; HD 158899, 11.754 Jy. We used the following Q_a fluxes for photometric calibration: HD 141992, 5.362 Jy; HD 158899, 4.650 Jy. [Photometric calibration fluxes from Cohen et al. (1999) and Gemini web pages.]

what smeared, so we measure photometry from only the “on” (guided) positions. Each “on” source has one half of the total integration time.

Three photometric calibrator stars [see Cohen et al. (1999) and the Gemini web pages³] were observed using the same observing mode (Tables 1 and 2). For each standard star, we measured the total flux using aperture photometry. The extinction we derived from these calibration measurements is consistent with zero.

The Eureka and 1998 VF₃₁ N' observations each were made with 24 total nods. For the Eureka observations, the image quality clearly degrades after the first 12 nods, so only these good quality images were used. For these data, we use a small centroided photometric aperture of 0.5 arcsec that is well matched to the size of the image. This small aperture reduces the sky background noise included in the photometric aperture, but requires an aperture correction. We derive an aperture correction of 1.62 by measuring fluxes from the standard stars with both large and small apertures. The final (aperture corrected) N' flux for Eureka is given in Table 2.

1998 VF₃₁ is somewhat fainter than Eureka, and is not visible in data from a single nod position. We used all 24 nod positions for this target, double-difference combined into three intermediate images of eight consecutive nod positions each. This allows us to make three independent measurements of the asteroid’s brightness. The final (aperture corrected) N' flux for 1998 VF₃₁ is given in Table 2.

At Q_a , Eureka is not visible in the data from individual nods nor easily visible in partial sums of the data. Consequently, we combine all the data into a single final double-differenced image. We used a small aperture of 0.7 arcsec, with an aperture correction of 1.23 (derived from the standard stars). The final (aperture corrected) Q_a flux for Eureka is given in Table 2.

We did not detect 1998 VF₃₁ at Q_a band and did not detect 2001 FR₁₂₇ at N' band. (Because 2001 FR₁₂₇ was not detected at N' , no measurement of that asteroid at Q_a was attempted.) To determine upper limits on the fluxes for these non-detections, we implanted scaled copies of the N' 1998 VF₃₁ point source in the 2001 FR₁₂₇ N' image and scaled copies of the Q_a Eureka point source in the 1998 VF₃₁ Q_a image. We measure the fluxes for the faintest implanted objects that are detected to set the up-

per limits for these two observations. These limits are roughly consistent with three times the sky noise (Table 2), as expected.

Eureka is the brightest asteroid source in our program, and we look to it to characterize the errors in our measurements. We have 12 independent measurements of Eureka at N' . The scatter in these flux measurements is comparable to the variation in the sky background (both around 12%). We therefore conclude that, for measurements where we have only few or one flux measurement and hence cannot characterize the scatter in the measurements, we can estimate the error in our measurement from the sky variability. We use this technique for both the 1998 VF₃₁ N' and Eureka Q_a measurements.

We convert Michelle counts to flux density units (mJy) by using the photometric calibrator stars (Table 2). We combine the measurements from all the calibrator stars to define a single calibration factor for each bandpass because the matches in time and sky location between calibration stars and asteroids are not very good. At N' , the calibration factor is uncertain at the 5% level, as estimated from the scatter among the calibration factors from the three standard star measurements; at Q_a , the uncertainty, derived the same way, is around 10%. We add these errors in quadrature with the errors in our measurements to derive the final errors reported in Table 2.

Our targets have temperatures around 250 K (as calculated in our thermal modeling, described below). Thus, color corrections can be important, as these asteroids are substantially colder than the calibrator stars (~ 4000 K). The isophotal wavelengths (wavelength at which the flux density from the object’s spectrum equals the average flux density calculated by integrating over the filter profile) for Ceres (217 K) in Michelle N' and Q_a are 11.52 and 18.26 μm , respectively (K. Volk, private communication). We adopt these Ceres isophotal wavelengths for our observed asteroids as our derived temperatures are quite close to the Ceres temperature used. We use these isophotal wavelengths in our thermal models described below, although these shifts from nominal wavelengths are relatively small and, compared to the errors in our measurements, unimportant.

5. Thermal modeling and model results

We interpret the observed thermal emission from our targets using the Standard Thermal Model (STM; e.g., Lebofsky and Spencer, 1989). The STM assumes a non-rotating (or zero thermal-inertia) spherical asteroid: dayside temperatures are

³ <http://www.gemini.edu/sciops/instruments/mir/MIRStdFluxes.html>.

in equilibrium with sunlight, while the nightside temperature is zero. Lebofsky et al. (1986) found that the thermal emission from asteroids frequently has a higher color temperature than would nominally be predicted under the STM assumptions given above, and introduced an empirical parameter, η , that allowed them to simultaneously model the elevated color temperature of the thermal emission and the (known) size of their targets (Ceres and Pallas). The canonical value for this beaming parameter η is 0.756, but recent studies (e.g., Harris, 1998; Delbó and Harris, 2002; Fernández et al., 2003; Stansberry et al., 2007) find that η can be significantly larger.

We rely on JPL’s Horizons ephemeris service for distance, phase angle, and absolute visual magnitude (H_V) information (Tables 1 and 2). We relate diameter, albedo, and H_V through

$$D = \frac{1329}{\sqrt{p_V}} \times 10^{-H_V/5}, \quad (1)$$

where p_V is the visible geometric albedo and D is the diameter in kilometers (Harris, 1998). We use a thermal phase coefficient 0.01 mag/deg. We assume standard scattering behavior for the surface in the visible, resulting in a phase integral $q = 0.39$.

Our data on Eureka allow us to determine the albedo p_V , diameter D , and beaming parameter η because Eureka is strongly detected at both N' and Q_a (in combination with H_V , this gives three measurements and three unknowns). Models with $\eta = 1.3$ give the best fit to the observed N' – Q_a color (Fig. 1), but η values in the range 0.57–2.45 are all formally consistent with the data and error bars given in Table 2. Using this range of η , we derive a diameter for Eureka of $1.28^{+0.44}_{-0.34}$ km. The corresponding albedo, when the diameter uncertainties and an uncertainty of 0.3 mag for H_V (Jurić et al., 2002; Romanishin and Tegler, 2005) are included, is $0.39^{+0.57}_{-0.23}$, a range of acceptable albedos that is so large as to be nearly useless. We take two approaches to generating more useful error bars.

Our first approach relies on results from other Solar System observing programs. Modeling of various Solar System observations has shown that the beaming parameter η is unlikely to have a value larger than ~ 1.8 (Fernández et al., 2003; Delbó et al., 2003, 2007; Stansberry et al., 2007). Requiring $\eta \leq 1.8$ reduces the upper bound on Eureka’s size and consequently the lower bound on the albedo, giving a diameter of $1.28^{+0.22}_{-0.34}$ km and an albedo of $0.39^{+0.57}_{-0.18}$ (including the uncertainty in H_V). Furthermore, Eureka’s albedo is unlikely to be larger than 0.5 (Harris and Lagerros, 2002; Delbó et al., 2003; Rivkin et al., 2007), which constrains the upper bound of the albedo and the lower bound of the diameter, giving $1.28^{+0.22}_{-0.29}$ km and an albedo of $0.39^{+0.11}_{-0.18}$.

Our second approach simply assigns $\eta = 1.3$ (the best fit for η) rather than using a range of η values. This gives a diameter of $1.28^{+0.08}_{-0.06}$ km and a resulting albedo of $0.39^{+0.18}_{-0.13}$ (with the uncertainty in H_V still included). We take these latter results as our derived best fits (Table 2), but emphasize that diameter and albedo both depend on choice of η , whose uncertainty is not captured in the error bars for this best fit, and that alternate assumptions produce different “best” results (as in our first approach). However, we note that in all cases the derived (and

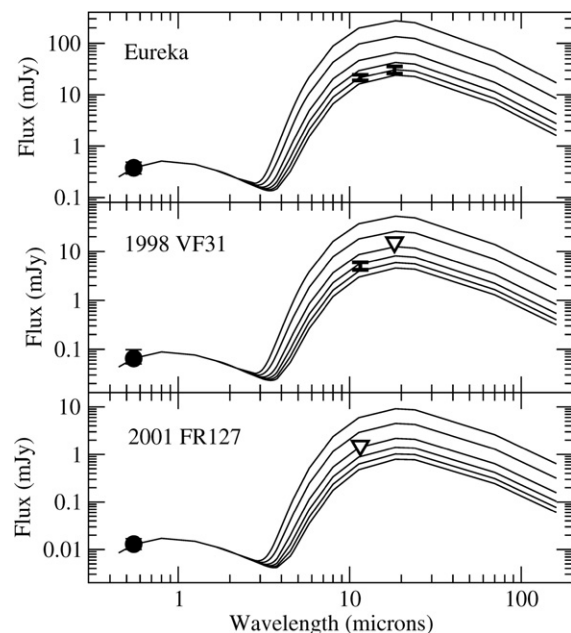


Fig. 1. Observed fluxes (plotted at isophotal wavelengths) and spectral energy distributions (solid curves) for the three observed Mars Trojans (as labeled), with STM solutions for a range of albedos and $\eta = 1.3$. Our detections are indicated by plotted error bars; upper limits are shown as downward pointing triangles. The isophotal wavelengths for these asteroids (temperatures around 250 K) are 11.52 and 18.26 μm for N' and Q_a , respectively (K. Volk, private communication). Data in the visible (circles) are taken from JPL’s Horizons service. (Error bars on the visible fluxes, corresponding to uncertainties in H of 0.3 mag, are shown, but are generally smaller than the symbol size.) Based on our lack of detection of photometric variation (lightcurve), we assign no extra scatter to the reflected light (visible) data. For each case, we derive diameters from thermal fluxes (assuming $\eta = 1.3$) and derive albedo from the derived diameter and known H_V . Here we show models that correspond to six albedos: 0.05, 0.10, 0.20, 0.30, 0.40, and 0.50, from top to bottom, respectively. These models assume the nominal H values for each asteroid; larger H values imply smaller albedos and smaller H values give larger albedos.

best-fit) albedo is consistent with the asteroid’s S(I) taxonomic class and interpreted angritic composition (Rivkin et al., 2007).

Drawing upon the success of the STM in fitting the Eureka data, we apply the STM with $\eta = 1.3$ to the data for 1998 VF₃₁ and 2001 FR₁₂₇; the results are shown in Fig. 1 and Table 2. This extrapolation of the STM to these other two bodies is warranted both because the sizes and temperatures of these three asteroids do not differ significantly, and because the available data for 1998 VF₃₁ and 2001 FR₁₂₇ are so sparse that they do not justify a different model. Because we have only a single mid-infrared data point for 1998 VF₃₁, we solve for the albedo and diameter (Table 2) simply by finding the STM solution that passes through the N' measurement. The errors on diameter give the range of solutions that are consistent with the 1σ photometric error bars; the albedo uncertainties include both the diameter uncertainty and 0.3 mag uncertainty in H_V . For 2001 FR₁₂₇, we solve for the maximum radius and minimum albedo by finding the STM solution that passes through the N' upper limit measurement. The lower limit on albedo here includes an uncertainty of 0.3 mag for H_V .

5.1. Eureka's thin regolith

Spencer et al. (1989) define the dimensionless thermal parameter Θ , which gives the ratio of the characteristic radiation timescale to the diurnal (rotation) timescale:

$$\Theta = \Gamma \left[\frac{(\omega R^3)^2}{\epsilon \sigma [(1-A) S_1]^3} \right]^{\frac{1}{4}}, \quad (2)$$

where Γ is the thermal inertia of the asteroid (units of $\text{J/m}^2/\text{K/s}^{1/2}$); ω is the rotational frequency ($\omega = 2 \times \pi/P$, where P is the rotational period); R is the heliocentric distance to the asteroid, in AU (Table 1); ϵ is the emissivity (we use $\epsilon = 0.9$); σ is the Stefan–Boltzmann constant; A is the bolometric albedo, which is $p_V \times q = 0.137$; and S_1 is the solar constant at 1 AU (we use 1366 W/m^2). For small asteroids with $\eta = 1.3$ and phase angle ~ 30 degrees, Γ is expected to be $200\text{--}400 \text{ J/m}^2/\text{K/s}^{1/2}$ and Θ is likely to be $1\text{--}2$ (Delbó, 2004; Delbó et al., 2007).

Rivkin et al. (2003) show a partial lightcurve for Eureka that suggests that Eureka's rotation period may be ~ 10 h. This period gives Θ of $1.6\text{--}3.2$ (for the above range of Γ), in good agreement with the expected value. Thus, Eureka's thermal properties appear to be consistent with theoretical expectations (Delbó, 2004) as well as with the results for similarly sized near-Earth objects (NEOs) (Delbó et al., 2007).

In the STM, dayside temperature goes as $\eta^{-1/4}$, so $\eta < 1$ results in warmer emission, while $\eta > 1$ results in cooler emission. Relatively cooler dayside temperatures will be produced by a high thermal inertia surface since some of the thermal emission will occur on the nightside. Our result that η is greater than unity is therefore consistent with our argument that Γ (thermal inertia) is relatively large. Both conclusions are consistent with a relative dearth of regolith, as predicted for bodies of this size (Binzel et al., 2004; Cheng, 2004), and with the small size we derive (e.g., Delbó et al., 2007). We note that relatively large η could also indicate a relatively smooth surface (on macroscopic scales), which again could imply a relatively thin regolith.

6. Summary and discussion

We observed the Mars Trojan Asteroids Eureka, 1998 VF₃₁, and 2001 FR₁₂₇ at N' ($11.2 \mu\text{m}$) and Q_a ($18.1 \mu\text{m}$). Using the Standard Thermal Model, we derive diameters (albedos) of 1.28 km (0.39), 0.78 km (0.32), and $<0.52 \text{ km}$ (>0.14), respectively. From several lines of argument, we conclude that Eureka's regolith is likely relatively thin, as predicted for a body this size. Eureka's thermal inertia is likely similar to that for comparably sized NEOs.

Rivkin et al. (2007) find that Eureka is angritic and that 1998 VF₃₁ appears to be an S(VII) (e.g., primitive achondrite) asteroid. In both cases, the albedos we derive are consistent with those taxa and implied compositions.

2001 FR₁₂₇ has a diameter ($<520 \text{ m}$) comparable to very small NEOs that have been observed in the mid-infrared (e.g., Delbó et al., 2003) and in radar experiments (e.g., Ostro et al.,

2002). These are among the smallest objects studied in the Solar System. By this virtue, further physical studies (spin, shape, lightcurve, etc.) are interesting on their own. Additionally, comparing physical properties between the dynamically old Mars Trojan asteroids studied here and the comparably sized but dynamically young NEOs may be useful in understanding the evolution of these smallest asteroids.

Acknowledgments

We thank Marco Delbó and Josh Emery for thoughtful, thorough, and helpful reviews. We thank Ed Olszewski and Grant Williams for their assistance with making 90prime observations. Marc Buie developed the IDL moving object pipeline that was used to detect and measure the position for 2001 FR₁₂₇. Larry Wasserman helped with the modification of this pipeline for other observational platforms and also provided useful input on positional errors for planning the 2001 FR₁₂₇ recovery observations. We thank Chad Engelbracht for helpful discussions about color corrections and Kevin Volk (Gemini) for providing the color corrections (isophotal wavelengths) for Michelle. We thank Tom Geballe, Scott Fisher, and Chad Trujillo (Gemini) and Rachel Mason and Michael Merrill (NOAO) for help with planning and carrying out the Gemini observations. This work is based in part on observations obtained at the Gemini Observatory, which is operated by the Association of Universities for Research in Astronomy, Inc., under a cooperative agreement with the NSF on behalf of the Gemini partnership: the National Science Foundation (United States), the Particle Physics and Astronomy Research Council (United Kingdom), the National Research Council (Canada), CONICYT (Chile), the Australian Research Council (Australia), CNPq (Brazil) and CONICET (Argentina). The data presented here were obtained under Gemini program GN-2005A-Q-47. We used the JPL Solar System Dynamics group's Horizons tool to plan our observations and analyze our results. This manuscript was prepared using the Elsevier/Icarus LaTeX template created by Ross Beyer et al. Finally, we are grateful to the indigenous people of Hawai'i for allowing astronomers to use their sacred mountain.

References

- Binzel, R.P., Rivkin, A.S., Stuart, J.S., Harris, A.W., Bus, S.J., Burbine, T.H., 2004. Observed spectral properties of near-Earth objects: Results for population distribution, source regions, and space weathering processes. *Icarus* 170, 259–294.
- Cheng, A.F., 2004. Collisional evolution of the asteroid belt. *Icarus* 169, 357–372.
- Cohen, M., Walker, R.G., Carter, B., Hammersley, P., Kidger, M., Noguchi, K., 1999. Spectral irradiance calibration in the infrared. X. A self-consistent radiometric all-sky network of absolutely calibrated stellar spectra. *Astron. J.* 117, 1864–1889.
- Delbó, M., 2004. The nature of near-Earth asteroids from the study of their thermal infrared emission. Ph.D. dissertation, FU Berlin. <http://www.diss.fu-berlin.de/2004/289/indexe.html>.
- Delbó, M., Harris, A.W., 2002. Physical properties of near-Earth asteroids from thermal infrared observations and thermal modeling. *Meteorit. Planet. Sci.* 37, 1929–1936.
- Delbó, M., Harris, A.W., Binzel, R.P., Pravec, P., Davies, J.K., 2003. Keck observations of near-Earth asteroids in the thermal infrared. *Icarus* 166, 116–130.

- Delbó, M., dell'Oro, A., Harris, A.W., Mottola, S., Mueller, M., 2007. Thermal inertia of near-Earth asteroids and implications for the magnitude of the Yarkovsky effect. *Icarus* 190, 236–249.
- Elliot, J.L., and 10 colleagues, 2005. The Deep Ecliptic Survey: A search for Kuiper Belt objects and Centaurs. II. Dynamical classification, the Kuiper Belt plane, and the core population. *Astron. J.* 129, 1117–1162.
- Fernández, Y.R., Sheppard, S.S., Jewitt, D.C., 2003. The albedo distribution of jovian Trojan asteroids. *Astron. J.* 126, 1563–1574.
- Glasse, A.C., Atad-Ettinger, E.I., Harris, J.W., 1997. Michelle midinfrared spectrometer and imager. *Proc. SPIE* 2871, 1197–1203.
- Harris, A.W., 1998. A thermal model for near-Earth asteroids. *Icarus* 131, 291–301.
- Harris, A.W., Lagerros, J.S.V., 2002. Asteroids in the thermal infrared. In: Bottke Jr., W.F., Cellino, A., Paolicchi, P., Binzel, R.P. (Eds.), *Asteroids III*. Univ. of Arizona Press, Tucson, pp. 205–218.
- Hergenrother, C.W., Trilling, D.E., Spahr, T.B., 2005. MPEC 2005-L35.
- Jurić, M., and 15 colleagues, 2002. Comparison of positions and magnitudes of asteroids observed in the Sloan Digital Sky Survey with those predicted for known asteroids. *Astron. J.* 124, 1776–1787.
- Lebofsky, L.A., Spencer, J.R., 1989. Radiometry and thermal modeling of asteroids. In: Binzel, R.P., Gehrels, T., Matthews, M.S. (Eds.), *Asteroids II*. Univ. of Arizona Press, Tucson, pp. 128–147.
- Lebofsky, L.A., Sykes, M.V., Tedesco, E.F., Veeder, G.J., Matson, D.L., Brown, R.H., Gradie, J.C., Feierberg, M.A., Rudy, R.J., 1986. A refined 'standard' thermal model for asteroids based on observations of 1 Ceres and 2 Pallas. *Icarus* 68, 239–251.
- Millis, R.L., Buie, M.W., Wasserman, L.H., Elliot, J.L., Kern, S.D., Wagner, R.M., 2002. The Deep Ecliptic Survey: A search for Kuiper Belt objects and Centaurs. I. Description of methods and initial results. *Astron. J.* 123, 2083–2109.
- Ostro, S.J., Hudson, R.S., Benner, L.A.M., Giorgini, J.D., Magri, C., Margot, J.-L., Nolan, M.C., 2002. Asteroid radar astronomy. In: Bottke Jr., W.F., Cellino, A., Paolicchi, P., Binzel, R.P. (Eds.), *Asteroids III*. Univ. of Arizona Press, Tucson, pp. 151–168.
- Rivkin, A.S., Binzel, R.P., Howell, E.S., Bus, S.J., Grier, J.A., 2003. Spectroscopy and photometry of Mars Trojans. *Icarus* 165, 349–354.
- Rivkin, A.S., Trilling, D.E., Thomas, C.A., DeMeo, F., Spahr, T.B., Binzel, R.P., 2007. Composition of the L5 Mars Trojans: Neighbors, not siblings. *Icarus* 192 (2), 434–441.
- Romanishin, W., Tegler, S.C., 2005. Accurate absolute magnitudes for Kuiper Belt objects and Centaurs. *Icarus* 179, 523–526.
- Scholl, H., Marzari, F., Tricarico, P., 2005. Dynamics of Mars Trojans. *Astron. Astrophys.* 175, 397–408.
- Spencer, J.R., Lebofsky, L.A., Sykes, M.V., 1989. Systematic biases in radiometric diameter determinations. *Icarus* 78, 337–354.
- Stansberry, J., Grundy, W., Brown, M., Cruikshank, D., Spencer, J., Trilling, D., Margot, J.-L., 2007. Physical properties of Kuiper Belt objects and Centaurs: Spitzer Space Telescope constraints. In: Barucci, A., Boehnhardt, H., Cruikshank, D., Morbidello, A. (Eds.), *The Kuiper Belt*. Univ. of Arizona Press, Tucson, in press.
- Tabachnik, S., Evans, N.W., 1999. Cartography for martian Trojans. *Astrophys. J.* 517, L63–L66.
- Tichy, M., and 16 colleagues, 2001. MPEC 2001-F58.
- Williams, G.G., Olszewski, E., Lesser, M.P., Burge, J.H., 2004. 90prime: A prime focus imager for the Steward Observatory 90-in. telescope. *Proc. SPIE* 5492, 787–798.